

Supplementary Information

In-situ formation of spherical MoS₂ nanoparticles for ultra-low friction

Kaiming Hou,^a Minmin Han,^a Xiaohong Liu,^a Jinqing Wang,^{*a} Yezeng He,^{*b} and

Shengrong Yang^{*a}

^aState Key Laboratory of Solid Lubrication, Lanzhou Institute of Chemical Physics,
Chinese Academy of Sciences, Lanzhou, 730000, China.

^bSchool of Materials Science and Engineering, China University of Mining and
Technology, Xuzhou, 221116, China.

Correspondence to jqwang@licp.cas.cn (J. Q. Wang) or to heyezeng@cumt.edu.cn (Y.
Z. He)

Supplementary Figures

Part 1 Characterization and analyses on morphology, structure and chemical compositions of Nano-MoS₂ coating.

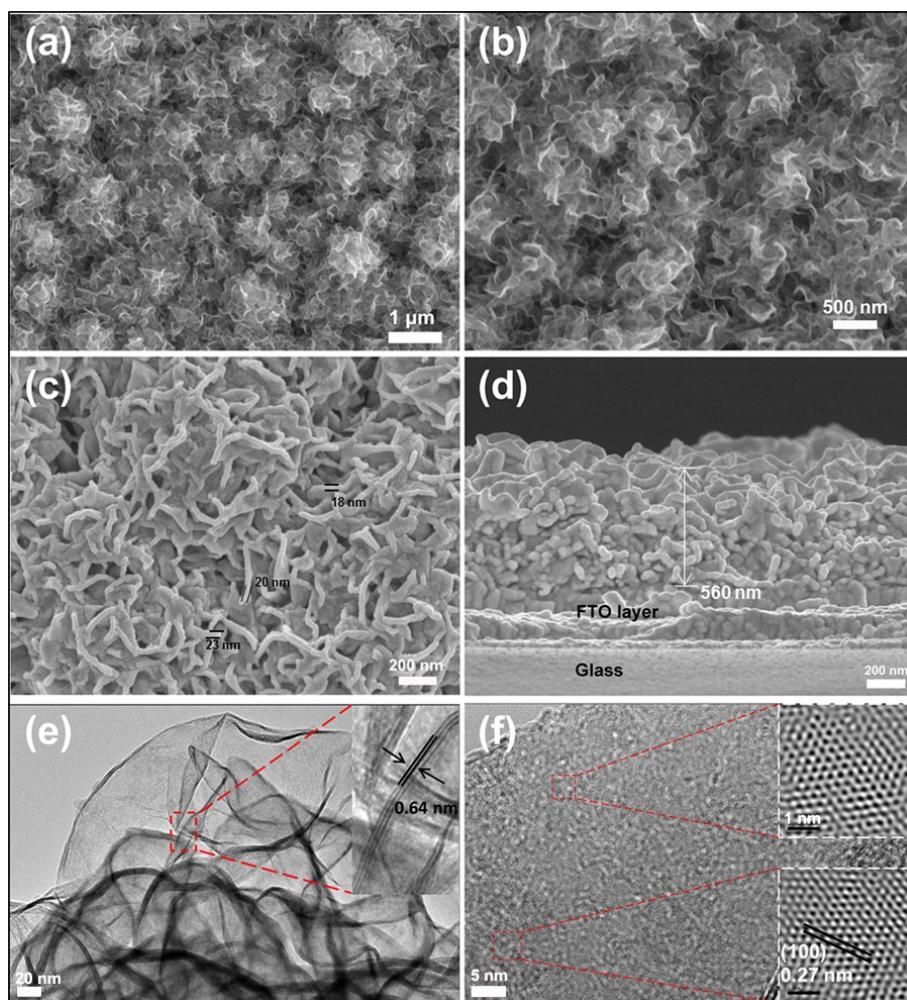


Fig. S1 Morphology and structure characterizations of Nano-MoS₂ coating. (a and b) Low magnified SEM images of Nano-MoS₂ coating. (c) High magnified SEM image, showing the nanosheet thickness of 24-26 nm. (d) The cross-sectional SEM image of the coating. (e) TEM image of the MoS₂ nanosheets, the inset shows the image of the region indicated by the red rectangle. (f) High resolution TEM image with the enlarged fast Fourier transform (FFT) pattern of selected region as shown in insets.

The low magnified scanning electron microscopy (SEM) images (as shown in Fig. S1a and b) show that Nano-MoS₂ coating obtained by hydrothermal process is

constituted of nanosheets continuously covering on the fluorine doped tin oxide (FTO) glass substrate. The thickness values of nanosheets vary from 24 to 26 nm (as shown in Fig. S1c). In Fig. S1d, the bonding of coating to substrate is founded to be tight and the thickness of coating is in the range of 550-600 nm. In the top and cross-sectional views, the Nano-MoS₂ coating all presents an open and loose structure as numerous nanosheets array disorderly. The ultrathin morphology of MoS₂ nanosheet is confirmed in the transmission electron microscopy (TEM) image (as shown in Fig. S1e). These nanosheets show large lateral dimension with a corrugated morphology. The curled edge further shows typical layered structure of MoS₂ with an interlayer spacing of 0.64 nm. In Fig. S1f, the high-resolution TEM image exhibits the well-defined crystal structure of MoS₂. A typical hexagonal structure can be seen, corresponding to a lattice spacing of 0.27 nm which can be assigned to the (100) planes.¹

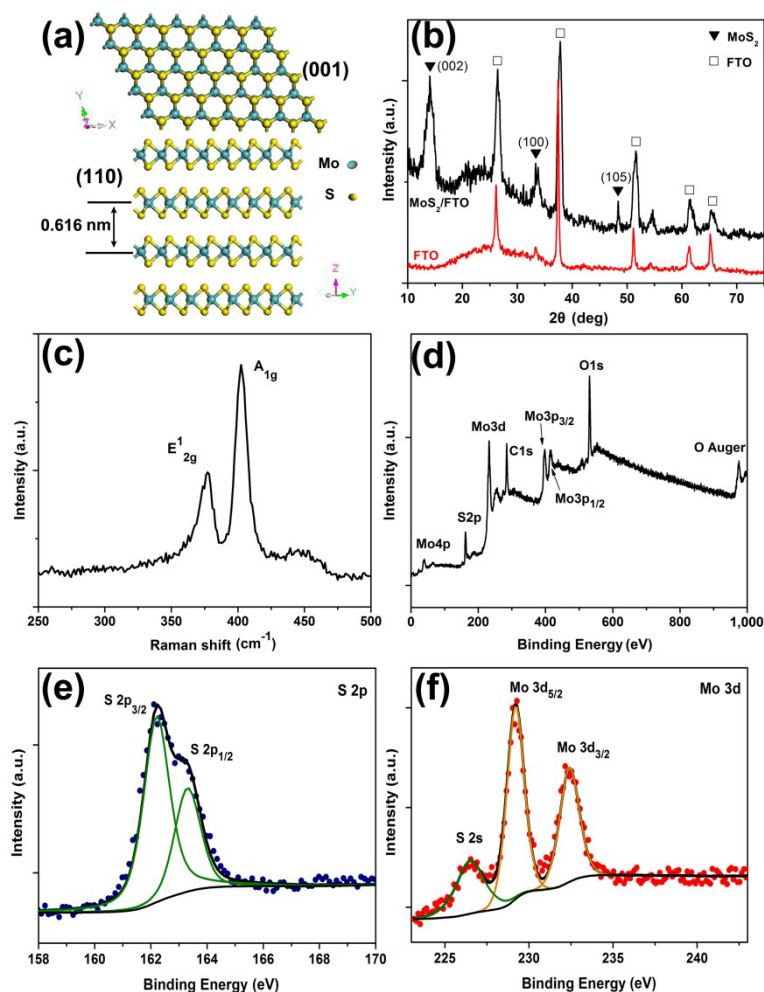


Fig. S2 Structure and chemical compositions analyses of Nano-MoS₂ coating. (a) Schematic illustrations of the (001) and (110) crystal planes for MoS₂. (b) Grazing incidence X-ray diffraction (XRD) patterns of Nano-MoS₂ coating grown on FTO glass. (c) Raman spectroscopy of coating sample using 514 nm laser line. The survey spectrum (d), Mo 3d (e) and S 2p (f) core level spectra of Nano-MoS₂ coating in X-ray photoelectron spectroscopy (XPS) characterizations.

Fig. S2a schematically illustrates the crystal structures of (001) and (110) planes for MoS₂. The hexagonal crystal contains a molybdenum atom layer covalently sandwiched between two layers of hexagonally packed sulfur atoms. The measured

interlayer spacing based on the position of (002) peak ($2\theta = 13.96^\circ$) in Fig. S2b is 0.636 nm, which is closed to the value of 0.616 nm for standard MoS₂ ($2\theta_{(002)} = 14.38^\circ$).² To characterize the chemical nature and bonding state of as-prepared Nano-MoS₂ coating, X-ray photoelectron spectroscopy (XPS) and Raman spectroscopy characterizations are performed. The Raman spectrum (Fig. S2c) shows the typical double peak signals of MoS₂ corresponding to the in-plane vibration E_{2g}¹ mode at 377 cm⁻¹ and the A_{1g} mode at 402 cm⁻¹.^{3,4} In the XPS survey spectrum, it is noted that the detected elements are Mo, S, C, and O elements (Fig. S2d). The C and O are from adventitious CO₂ and water vapor, etc. adsorbed instead of molybdenum oxide. The carbon peak (284.8 eV) is taken as a reference to calibrate the data. The S 2p core level spectra (Fig. S2e) exhibit a clear doublet S 2p_{1/2} and S 2p_{3/2} at 163.3 and 162.2 eV respectively by deconvolution. There is no broad oxidation peak at 168-170 eV, suggesting no oxidation occurs. In the deconvoluted Mo 3d core level spectra (Fig. S2f), the peaks at 229.2 and 232.5 eV are corresponded to the Mo 3d_{5/2} and Mo 3d_{3/2} for Mo⁴⁺. A small peak located at lower binding energy of 226.5 eV is assigned to S 2s. The absence of Mo⁶⁺ 3d_{5/2} at around 236 eV indicates that the sample remains unoxidized.⁵⁻⁷

Part 2 The tribological performances of Nano-MoS₂ coating under different sliding velocities.

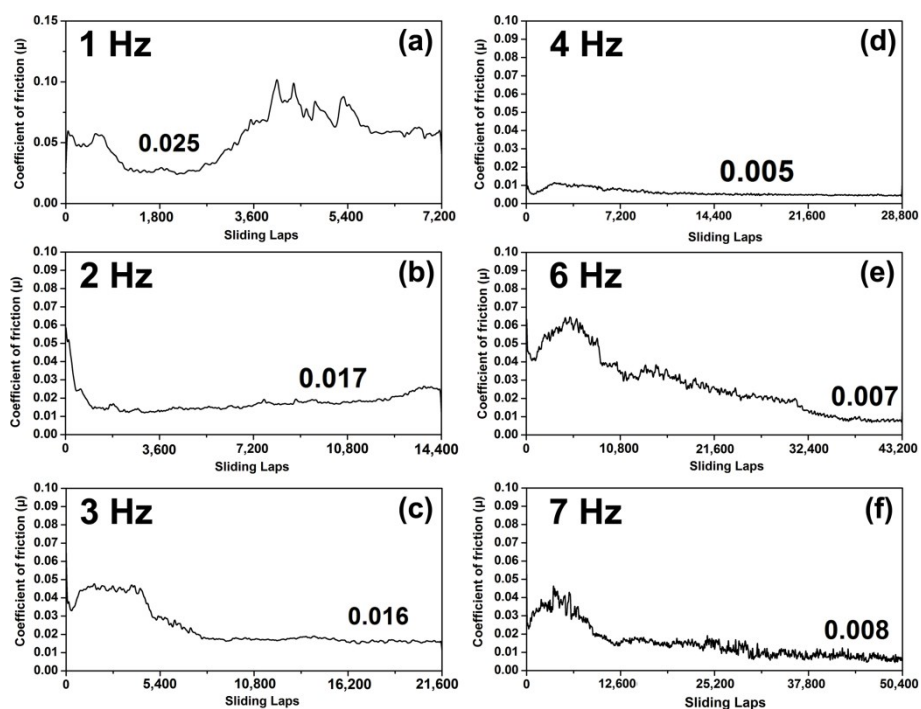


Fig. S3 The friction performances of Nano-MoS₂ coating under different sliding velocities. The friction curves of Nano-MoS₂ coating under low loads of 0.5 N and various sliding velocities in the range of 1 to 7 cm/s (corresponding to the 1-7 Hz).

In the sliding velocities ranging from 1 to 3 cm/s, the friction coefficients show a decrease trend. When the sliding velocity is 4 cm/s, the ultra-low friction can be achieved with a smooth running curve. Further increasing the sliding velocity to 6 and 7 cm/s, the ultra-low friction can also be achieved at the late stage of test. However, the friction curves present fluctuations, suggesting an unstable lubrication state.

Part 3 The chemical composition of spherical nanoparticle.

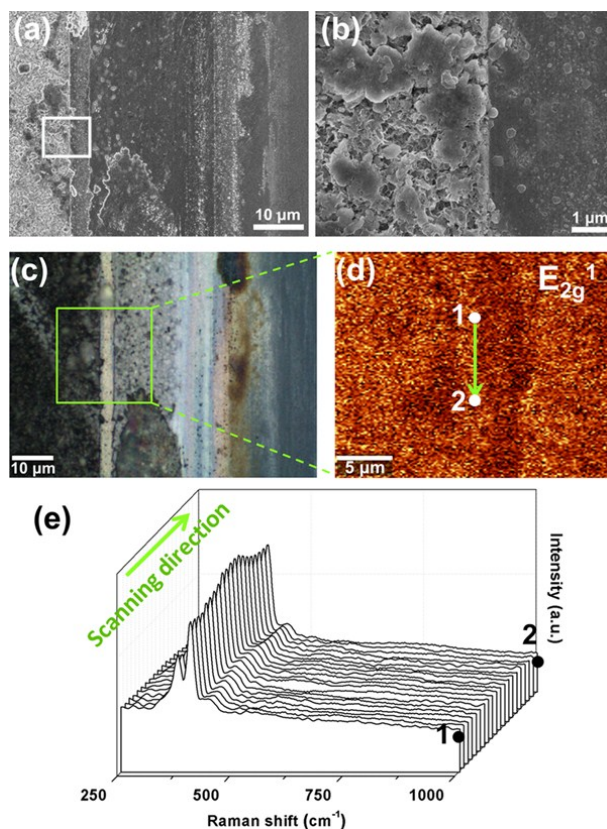


Fig. S4 The Raman mapping analysis of wear track. (a) The SEM image of wear track on Nano-MoS₂ coating. (b) The enlarged image of the region indicated by the white rectangle in (a). (c) The optical photo of wear track. (d) Raman mapping of the characteristic E_{2g}¹ peak for MoS₂ in the selected region. (e) The Raman spectra collected along the scanning direction indicated by the green arrow in (d).

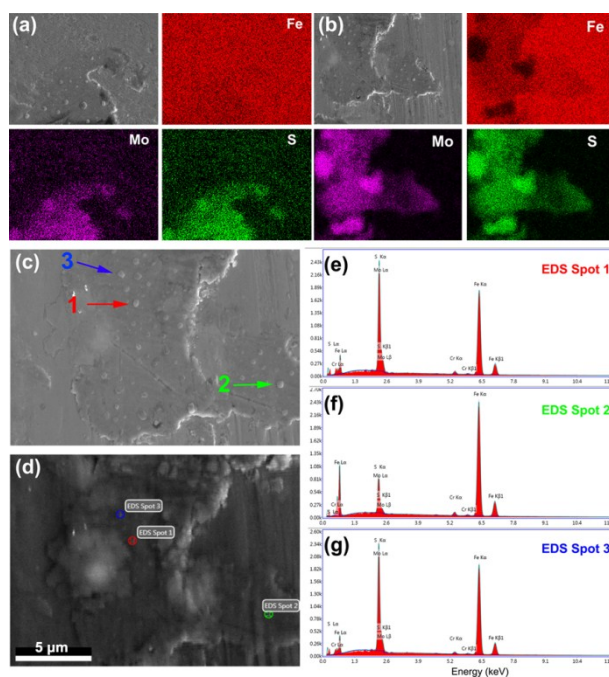


Fig. S5 Chemical composition analyses of spherical nanoparticles by EDS. EDS mapping analyses of the wear scars tested under 0.5 N (a) and 1.0 N (b). (c) The SEM image of selected area for EDS spot analysis. (d) The blurred image acquired under EDS detection mode for the same area, three specific positions are chosen corresponding to the locations of MoS₂ nanoparticles. The obtained EDS spectra from (e) to (g) indicate the Mo and S are detected together with Fe, Si and Cr elements from steel.

In the EDS mapping analyses (Fig. S5a and b), the MoS₂ is found to cover the area where spherical nanoparticles are distributed. EDS spot analyses (Fig. S5c-g) suggest that apart from the elements (Fe, C, and Si) from steel substrate, only Mo and S element are detected with S/Mo ratios ranging from 2.0 to 2.15 in the detection spots corresponding to the locations of spherical nanoparticles. This also confirms that the chemical composition of spherical nanoparticle is MoS₂.

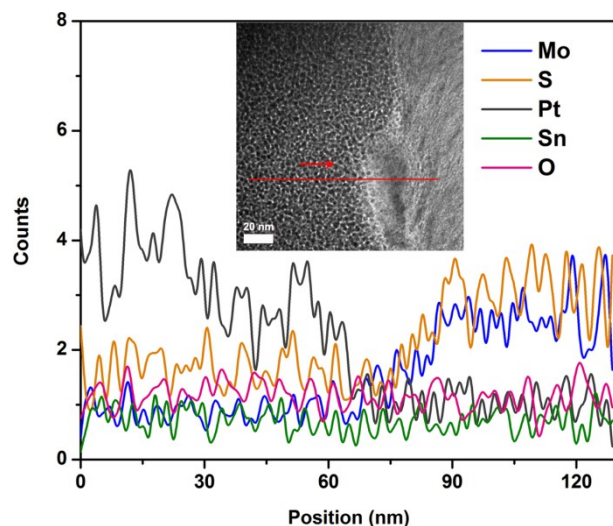


Fig. S6 EDS line scanning analysis to a specific spherical nanoparticle.

To further confirm the chemical composition of spherical nanoparticle observed on wear scar, EDS line scanning analysis is conducted on the sample obtained by FIB milling. The inset in Fig. S6 is the TEM image and the elemental signal is detected along the red line. The platinum (Pt) signal is ascribed to the protective Pt layer deposited on the top of sample before milling. The Pt signal intensity decreases when the detection position reaches the spherical nanoparticle, while the Mo and S signals gain intensity at the same position. Other possible contamination elements such as Sn and O have no any change, suggesting the chemical compositions of spherical nanoparticle are Mo and S.

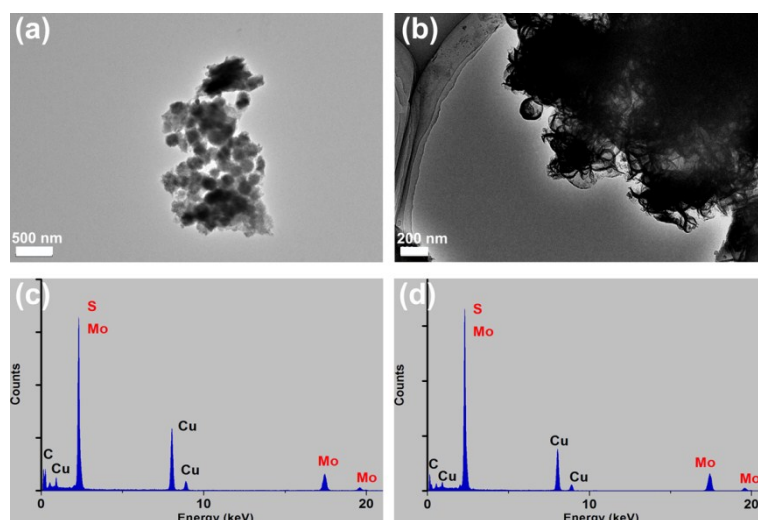


Fig. S7 TEM and EDS characterizations of the wear debris containing spherical nanoparticles and fragments of MoS₂ nanosheets. (a and b) The TEM images of wear debris. (c and d) The obtained EDS spectra of samples in (a) and (b) respectively.

TEM and EDS characterizations of the wear debris are performed as shown in Fig. S7. In the TEM image of Fig. S7a, the spherical morphology of MoS₂ nanoparticles can be seen together with some fragments of MoS₂ nanosheets. But due to the large size, these spherical nanoparticles are not transparent to the electron beam, which makes it impossible to observe the interior structure. Only at the edge of the debris, thin regions show electron transparency as shown in Fig. S7b. The EDS spectra (Fig. S7c and d) provide chemical composition information of the nanoparticles with only Mo and S elements.

Part 4 The characterization and tribological performance of PLD-MoS₂ coating.

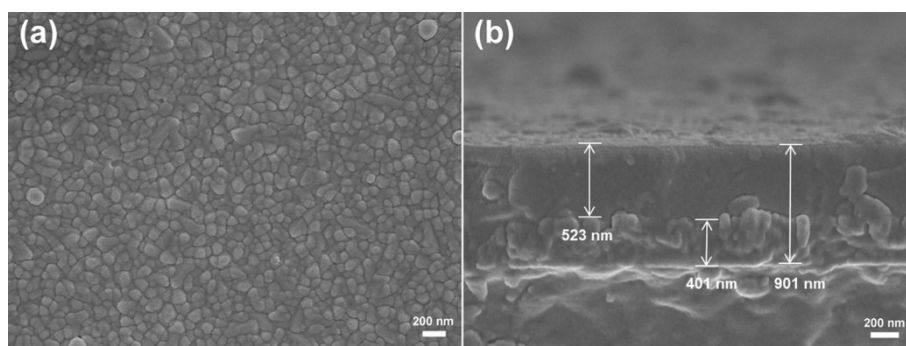


Fig. S8. Morphology and structure characterization of PLD-MoS₂ coating. The top view (a) and the cross-sectional view (b) of PLD-MoS₂ coating.

As control, the PLD-MoS₂ coating is prepared and observed by SEM as shown in Fig. S8. In the top view of PLD-MoS₂ coating (Fig. S8a), the continuously distributed granular bulges are the top of columnar crystals which is a typical microstructure in polycrystalline thin film prepared by low-temperature deposition.⁸ The PLD-MoS₂ coating is dense and well-adherent on substrate in the cross-sectional view (Fig. S8b). The thickness of PLD-MoS₂ coating is ~525 nm, which is close to the value of Nano-MoS₂ coating.

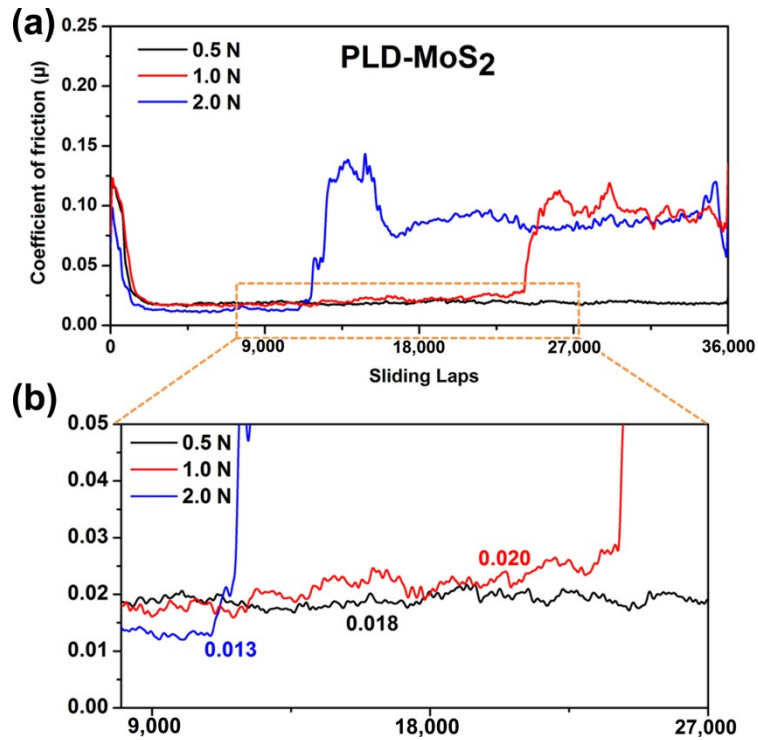


Fig. S9 The friction performances of PLD-MoS₂ coating. The coefficient of friction as a function of sliding laps for PLD-MoS₂ coating under the normal loads of 0.5, 1.0 and 2.0 N in vacuum test.

Compared with Nano-MoS₂ coating, the PLD-MoS₂ coating shows higher μ values in the range of 0.013-0.02 under the same tribological test conditions. Moreover, the robustness and durability of PLD-MoS₂ coating are weaker as the Nano-MoS₂ coating can sustain the load of 1.0 N during the whole test process while the lubrication failure occurs after 24000 sliding laps for PLD-MoS₂ coating. Under the load of 2.0 N, PLD-MoS₂ coating has a wear life of only ~11000 sliding laps while the wear life of Nano-MoS₂ coating is up to 22000 laps.

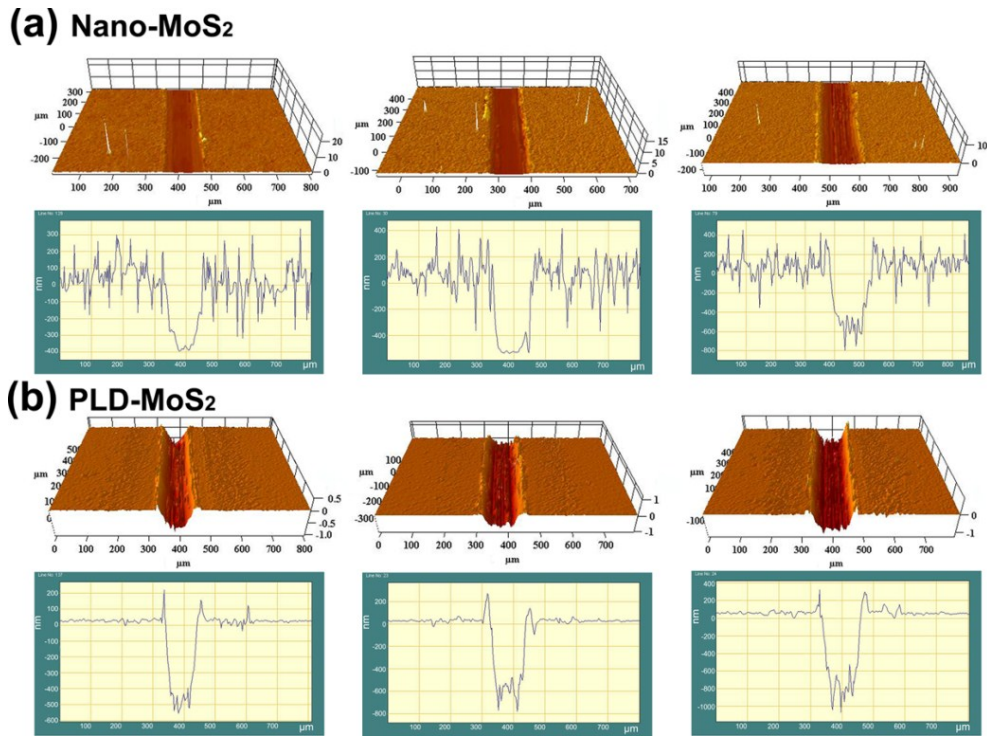


Fig. S10 The comparison of wear between Nano-MoS₂ coating and PLD-MoS₂ coating. The three-dimensional optical microscopic images of wear tracks (top images) and corresponding cross-sectional profiles (bottom images) for Nano-MoS₂ coating (a) and PLD-MoS₂ coating (b) under 0.5, 1.0 and 2.0 N (from left to right).

The wear depths for Nano-MoS₂ coating are less than the coating thickness and the bottom surfaces of wear tracks are relatively flat under 0.5 and 1 N, revealing a good accommodation in the contact geometry (Fig. S10a). Opposed to this, the wear tracks on PLD-MoS₂ coating all have clear grooves and scratches. Except in the case of 0.5 N, the wear depths are all larger than the coating thickness, suggesting the direct asperity contact occurs (Fig. S10b). This asperity contact leads to the rapid increase of friction coefficient in Fig. S9. We estimate this performance difference is associated with the specific microstructure of MoS₂ coating. The Nano-MoS₂ coating can distribute the stress by deformation and reorientation of nanosheets; however, the

dense PLD-MoS₂ coating causes localized stress which can be further transmitted along the vertically aligned columnar crystals to the bottom of coating.⁹

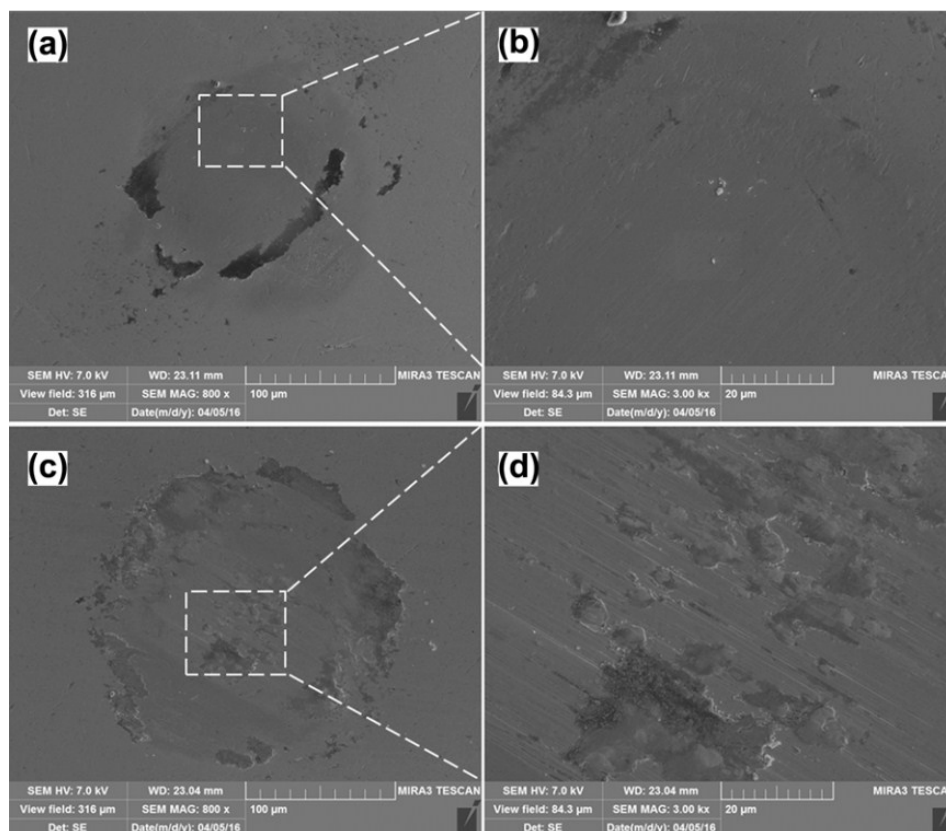


Fig. S11 The stepwise magnified SEM images of wear scars on steel ball after sliding against PLD-MoS₂ coating. The wear scar images obtained under the load of 0.5 N (a and b) and 1.0 N (c and d).

Fig. S11 shows the stepwise magnified SEM images of wear scars on steel ball after sliding against PLD-MoS₂ coating under the loads of 0.5 and 1.0 N. Under the load of 0.5 N (Fig. S11a and b), there is only transfer film observed and no any spherical particle presents on the wear scar surface. In vacuum, as a common feature, the formation of transfer film is the dominant factor for MoS₂ lubrication. When the load increases to 1.0 N (Fig. S11c and d), apart from the transfer film, obvious groove

and scratches are observed at the central area of wear scar, corresponding to the direct asperity contact between steel ball and FTO glass.

References

1. X. Huang, Z. Zeng, S. Bao, M. Wang, X. Qi, Z. Fan and H. Zhang, *Nat. Commun.*, 2013, **4**, 1444.
2. R. G. Dickinson and L. Pauling, *J. Am. Chem. Soc.*, 1923, **45**, 1466-1471.
3. H. Li, Q. Zhang, C. C. R. Yap, B. K. Tay, T. H. T. Edwin, A. Olivier and D. Baillargeat, *Adv. Funct. Mater.*, 2012, **22**, 1385-1390.
4. A. P. Nayak, T. Pandey, D. Voiry, J. Liu, S. T. Moran, A. Sharma, C. Tan, C. H. Chen, L. J. Li, M. Chhowalla, J. F. Lin, A. K. Singh and D. Akinwande, *Nano Lett.*, 2014, **15**, 346-353.
5. K. C. Knirsch, N. C. Berner, H. C. Nerl, C. S. Cucinotta, Z. Gholamvand, N. McEvoy, Z. Wang, I. Abramovic, P. Vecera, M. Halik, S. Sanvito, G. S. Duesberg, V. Nicolosi, F. Hauke, A. Hirsch, J. N. Coleman and C. Backes, *ACS Nano*, 2015, **9**, 6018-6030.
6. G. Eda, H. Yamaguchi, D. Voiry, T. Fujita, M. Chen and M. Chhowalla, *Nano Lett.*, 2011, **11**, 5111-5116.
7. A. S. George, Z. Mutlu, R. Ionescu, R. J. Wu, J. S. Jeong, H. H. Bay, Y. Chai, K. A. Mkhoyan, M. Ozkan and C. S. Ozkan, *Adv. Funct. Mater.*, 2014, **24**, 7461-7466.
8. I. Petrov, P. B. Barna, L. Hultman and J. E. Greene, *J. Vac. Sci. Technol. A*, 2003, **21**, 117-128.
9. K. Sugimoto, K. Matsui, T. Okamoto and K. Kishitake, *Trans. JIM*, 1975, **16**, 647-655.